Journal of Applied Polymer Science

Thermal, Electrical, and Mechanical Properties of Tween 80/Span 80-Based Organogels and Its Application in Iontophoretic Drug Delivery

Sai S. Sagiri, Uttam Kumar, Biswajeet Champaty, Vinay K Singh, Kunal Pal
Department of Biotechnology and Medical Engineering, National Institute of Technology, Rourkela-769008, Odisha, India
Correspondence to: K. Pal (E-mail: pal.kunal@yahoo.com)

ABSTRACT: The present study describes the preparation and characterization of the Tween 80/Span 80 and sunflower oil–based organogels. Organogels were characterized using microscopy, X-ray diffraction, thermal, mechanical, and electrical techniques. The properties were found to be dependent on the proportion of the water : surfactant mixture. The *in vitro* drug release studies were performed under electrical potential. The drug release in the presence of electrical current was compared with the passive drug release. The drug release from the organogels followed the zero-order kinetics suggesting diffusion mediated release. The preliminary results suggested that the organogels may be used as drug carriers in iontophoretic drug delivery. © 2014 Wiley Periodicals, Inc. J. Appl. Polym. Sci. **2015**, *132*, 41419.

KEYWORDS: biocompatibility; drug delivery systems; gels

Received 29 June 2014; accepted 18 August 2014
DOI: 10.1002/app.41419

INTRODUCTION

Skin is the largest organ and the integumentary system of the body.[1] It has been extensively explored to deliver drugs either to elicit pharmacological actions either locally or systemically.[2] The delivery of drugs into the systemic circulation across the skin is regarded as transdermal delivery. The main advantage of transdermal drug delivery is bypassing the first-pass metabolism by the drug molecules. But the migration of the drug from the skin surface into the systemic circulation is the rate-limiting step.[3] Many approaches (e.g., use of permeation enhancers, electrical energy, ultrasound or a combination of these) have been adopted to improve the permeation of the drugs through the skin layer.[4] Among the techniques studied, iontophoretic drug delivery system has evolved as one of the widely explored transdermal drug delivery systems. Iontophoresis is a non-invasive transdermal drug delivery methodology which uses a low intensity electric current to promote permeation of the drug across the skin.[5] The method is based on the phenomenon of "like charges repel each other".[6] The technique uses a two-electrode system. One of the electrodes is the active electrode, whereas, the other is the passive electrode. The drug molecules used for iontophoretic drug delivery are usually charged molecules.[7] But various neutral drug molecules have also been tried.[8] If the drug molecules are anionic in nature then cathode is made as the active electrode and vice versa.[9] The delivery of the drug has been found to be dependent on the profile of the electric current applied. Various current profiles have been applied and their effect on the release profile has been studied extensively.[10,11]

Drugs are usually incorporated within gel based matrices. The drug loaded matrices are placed in the donor compartment. The matrices should be electrically conductive in nature.[12–14] Till recent past, only hydrogels were regarded as suitable for iontophoretic delivery systems.[15–18] Of late, water containing organogels are being explored as delivery matrices for iontophoretic drug delivery.[14] Organogels are gel based systems which immobilizes apolar solvents.[19] In general, organogels are electrically non-conductive.[20,21] Organogel based formulations may be designed to contain pockets of water, which can make the organogels electrically conductive.[22] Even though water pocket containing organogels have suitable properties to be used in iontophoretic drug delivery, only few studies have been reported which explore the suitability of the organogels for iontophoretic drug delivery. Taking a note of this, we have tried to thoroughly characterize Tween 80-Span 80 based organogels (previously reported by our group) to determine its suitability as iontophoretic delivery vehicles.[23]

MATERIALS AND METHODS

Materials

Basic electronic components were procured from the local market. Microprocessor (SPEEDY-33) was purchased from National Instruments, USA. Span 80 (sorbitan monooleate; SM) was

© 2014 Wiley Periodicals, Inc.

Table I. Composition of the Organogels

Samples	Composition % (w/w) SM	DW	SO	SA % (w/w)	DW/SM ratio
F1	50.0	20.0	30.0	—	0.40
F2	60.0	20.0	20.0	—	0.30
F3	50.0	30.0	20.0	—	0.60
F1D	49.5	20.0	30.0	0.5	0.404
F2D	59.5	20.0	20.0	0.5	0.336
F3D	49.5	30.0	20.0	0.5	0.606

purchased from Loba Chemie, Mumbai, India. Tween 80 (polyoxyethylene sorbitan monooleate; PM) and sodium salicylate (SA) were purchased from HiMedia, Mumbai, India. The stainless steel (SS) electrodes for the iontophoretic studies were fabricated using high quality SS plates. Edible grade refined sunflower oil (SO) was procured from the local market. All the studies were conducted using double distilled water.

Preparation of Organogels

The preparation of the organogels was performed by fluid filled fiber mechanism as per the previously reported literature.[19] Surfactant mixture of SM-PM (1 : 2 weight ratio) was used as the organogelator. The organogels were prepared by altering the compositions of SM-PM, sunflower oil and water. The compositions of the selected organogels have been provided in Table I. In brief, SM-PM mixture was dissolved in sunflower oil and subsequently homogenized using magnetic stirrer (100 rpm) at room-temperature (RT, 25°C). To this homogenized solution, water was added drop-wise with continuous vortexing. After the addition of water, the mixture was vortexed further for 3 min. Drug containing organogels were prepared using sodium salicylate solution in water as the aqueous phase. The final concentration of the drug in the formulations was kept 0.5% w/w.

Microscopic Studies

The microscopic evaluation of the organogels was performed using bright field microscope (Leica-DM750 equipped with ICC 50-HD camera, Germany) and scanning electron microscope (SEM, JEOL, JSM-6390, Japan). SEM analysis was performed using xerogels. The organogels were converted into xerogels as per the reported literature.[24] The xerogels were subsequently sputter-coated with platinum, before visualization under the SEM.[25]

Thermal Studies

Differential scanning calorimeter (DSC-200 F3 MAIA, Netzsch, Germany) was used to study the thermal properties of the organogels. The organogels were scanned in the temperature range of 20–150°C at a scan rate of 2°C/min under N_2 environment in aluminum (Al) pans with pierced Al lid. Accurately weighed 15–20 mg of the organogels were taken in Al pans and hermetically sealed with Al lids.

Impedance Measurement

The electrical properties of the organogels were measured using a computer-controlled impedance analyzer (Phase sensitive multimeter, Model: PSM1735, Numetriq, Japan) in the frequency range of 0.1 Hz to 1.0 MHz.[26]

Mechanical Analysis

Mechanical properties of the organogels were determined using a static mechanical tester (Stable Microsystems, TA-HD plus, U.K.). The stress relaxation, gel strength, spreadability and backward extrusion studies were performed at RT. Table II summarize the details of the mechanical studies.[27,28]

Viscosity Studies

Viscoelastic properties of the organogels were studied by using a cone (cone angle: 5.4° and diameter: 30 mm) and plate viscometer (Bohlin Visco 88, Malvern, UK). All the viscosity studies were conducted at RT.[29]

In Vitro Drug Delivery

The drug delivery studies were performed using a specially designed diffusion cell (Figure 1). SS plates (diameter: 2 cm) were used as the electrodes and were connected to the donor and the dummy chambers. The donor chamber contained drug loaded organogel, whereas the dummy chamber contained normal saline (Figure 1). The donor chamber was separated from the receptor chamber using a pre-activated dialysis membrane. The experimental set-up of the iontophoretic drug delivery

Table II. Details of Texture Analysis Studies

Type of study	Type of fixture	Testing conditions Pretest speed (mm/sec)	Test speed (mm/sec)	Post-test speed (mm/sec)	Mode of study
Stress relaxation	HDP/SR spreadability rig with 45° conical perspex probe	1.0	0.5	10.0	Auto force (5 g, 5 mm)
Gel strength	P/3 30mm diameter cylindrical probe	1.0	1.0	10.0	Button mode (30 mm)
Spreadability	HDP/SR spreadability rig with 45° conical perspex probe	2.0	2.0	2.0	Auto force (5 g, 20 mm)
Backward extrusion	A/BE back extrusion rig	1.0	1.0	1.0	Buttonmode

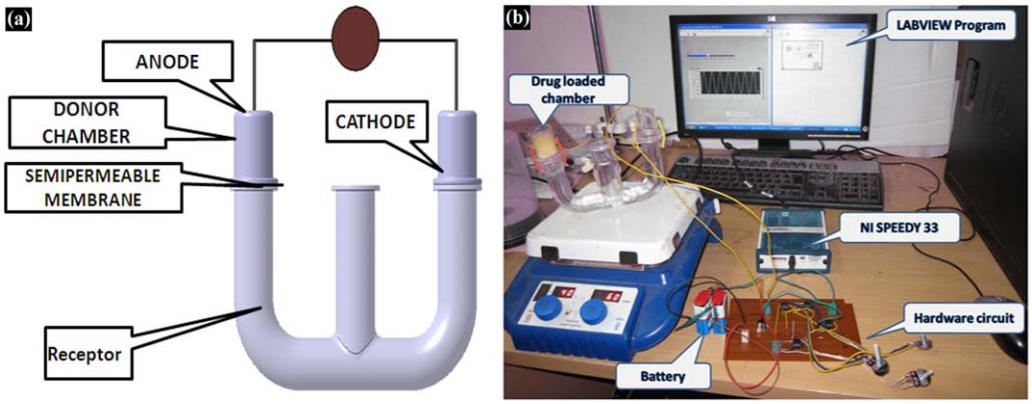

Figure 1. (a) Schematic sketch of iontophoretic set up and (b) experimental setup of iontophoretic drug delivery system. [Color figure can be viewed in the online issue, which is available at wileyonlinelibrary.com.]

system has been shown in Figure 1(b). SPEEDY-33 was used for the generation of the basic waveforms (e.g., sinusoidal and square) and was controlled by a LabVIEW program. The current flowing through the system was 1.06 mA, which provided a current density of 0.048 μA/cm^2. The effect of application of various waveforms on the release profile of the drug was studied (Table III). The study was conducted for 4 h. Three milliliters of the receptor volume was sampled at regular intervals of time (15 min during the first hour and 30 min thereafter). Three milliliters of the receptor volume was replaced with fresh water. The samples were then analyzed spectrophotometrically using a UV-visible spectrophotometer (UV-3200, LabIndia, Mumbai, India) at a λ_{max} of 294 nm.[30,31]

RESULTS AND DISCUSSION

Preparation of Organogels

The solution of SM-PM mixture in sunflower oil was light brown in color. Addition of water resulted in the formation of yellowish white or milky white colored semi-solid formulations (Figure 2). An increase in the water proportion resulted in the apparent increase in the whiteness of the formulations. On the other hand, an increase in the SM-PM proportion resulted in the formation of gels with higher yellowish tinge. The formation of organogels was confirmed by inverted test-tube method.[32] The formulations were regarded as organogels when they did not flow under gravity [Figure 2(b)]. Stable gels were also formed after loading sodium salicylate into the organogels. The pHs of the developed organogels were in the range of 6.0–7.0. The bright field microscopy of the organogels showed presence of droplets of water within an oil continuum phase [Figure 2(a)]. The droplets of water were stabilized by the SM-PM layer, which formed a protective layer at the interface of the water and sunflower oil. The droplets were interconnected to form a three-dimensional network structure. The FTIR studies suggested presence of the intermolecular hydrogen bonding among the organogel components (results not shown). This has been a usual phenomenon in water containing organogels.[22,33–35] Sodium salicylate loaded organogels showed the presence of peaks associated with the aromatic ring of the drug. There were no specific interactions among the gel components and the drug molecules. X-ray diffraction (XRD; results not shown) showed a broad diffraction peak at 20° 2θ thereby suggesting the amorphous nature of the organogels.[24] The crystallinity of the organogels, as predicted from the XRD profiles, was in the order of F3> F2>F1.

SEM Studies

The xerogels were visualized under SEM and have been shown in Figure 3. The microstructure showed the presence of fibrous structures of organogelators. Addition of water to the solution of SM-PM in sunflower oil resulted in the organization of the surfactant molecules to form inverse micelles. These inverse micelles formed 3D mesh-like structure which, in turn, resulted in the immobilization of sunflower oil.[36] The microstructure of the xerogels was dependent on the composition of the organogels. All the three formulations showed the presence of gelator fibers, but of different architectures. Reverse micellar structures were distinctly visible in F2 and F3. F1 showed the presence of predominantly spherulitic structures. In addition to the reverse micellar structures, F3 also showed the presence of spherulitic arrangements. The presence of reverse micellar structures was

Table III. Basic Waveforms Used in Iontophoretic Drug Delivery

Basic waveform	Amplitude of basic waveform (V_{pp})	Frequency of basic waveform (Hz)	Signal conditioning circuit	Modulated waveform
Sinusoidal	3.00	440	—	SN
Square	3.00	440	—	SQ
Sinusoidal	3.00	440	Half-wave rectifier	SNH
Square	3.00	440	Half-wave rectifier	SQH (pulsed DC)

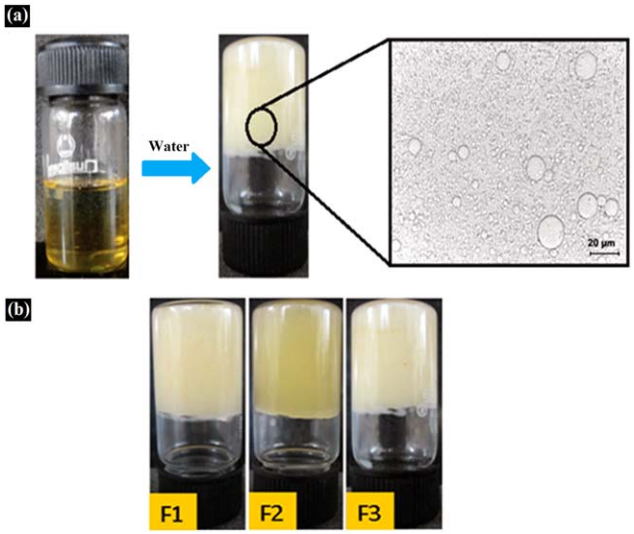

Figure 2. (a) Formation of organogels showing BFM image and (b) the stable organogels. [Color figure can be viewed in the online issue, which is available at wileyonlinelibrary.com.]

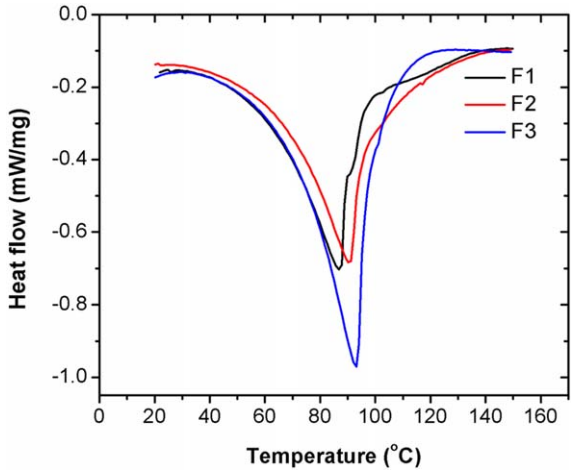

Figure 4. DSC thermograms of organogels. [Color figure can be viewed in the online issue, which is available at wileyonlinelibrary.com.]

not predominant in F3 as was in F2 formulation. The formation of predominant reverse micellar structures in F2 might be accounted to the lower water to SM-PM ratio (DW/SM-PM). Because the DW/SM-PM ratio was highest in F3, spherulitic arrangement of fibers was seen [Figure 3(c)]. Formation of spherulites in these organogels was by heterogeneous nucleation mechanism as evident by the radial outgrowth of gelator fibers from the nucleation point.[37] The microstructure of the organogels as observed under light microscopy and SEM are different from each other. This may be explained by the fact that there are chances of alteration of original micro-architecture because of the molecular rearrangements of the organogel components while extracting out the apolar continuum phase. The 3D architecture is often reported to collapse upon itself during conversion to xerogels.[38]

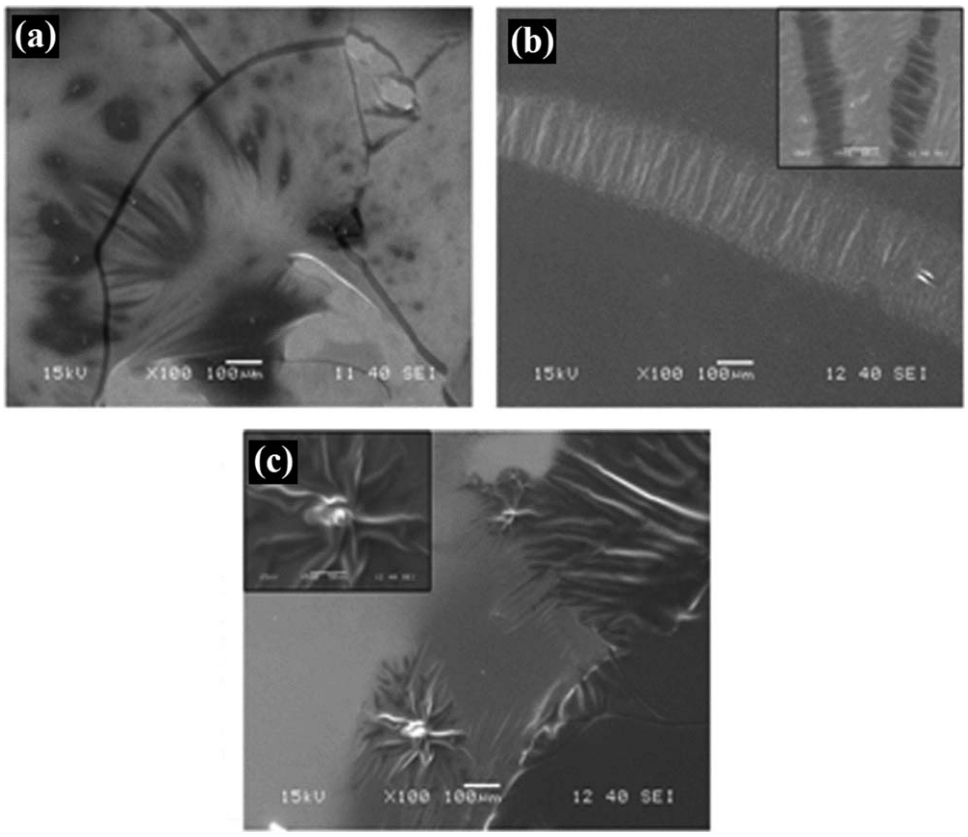

Figure 3. SEM images of the (a) F1, (b) F2, and (c) F3 organogels.

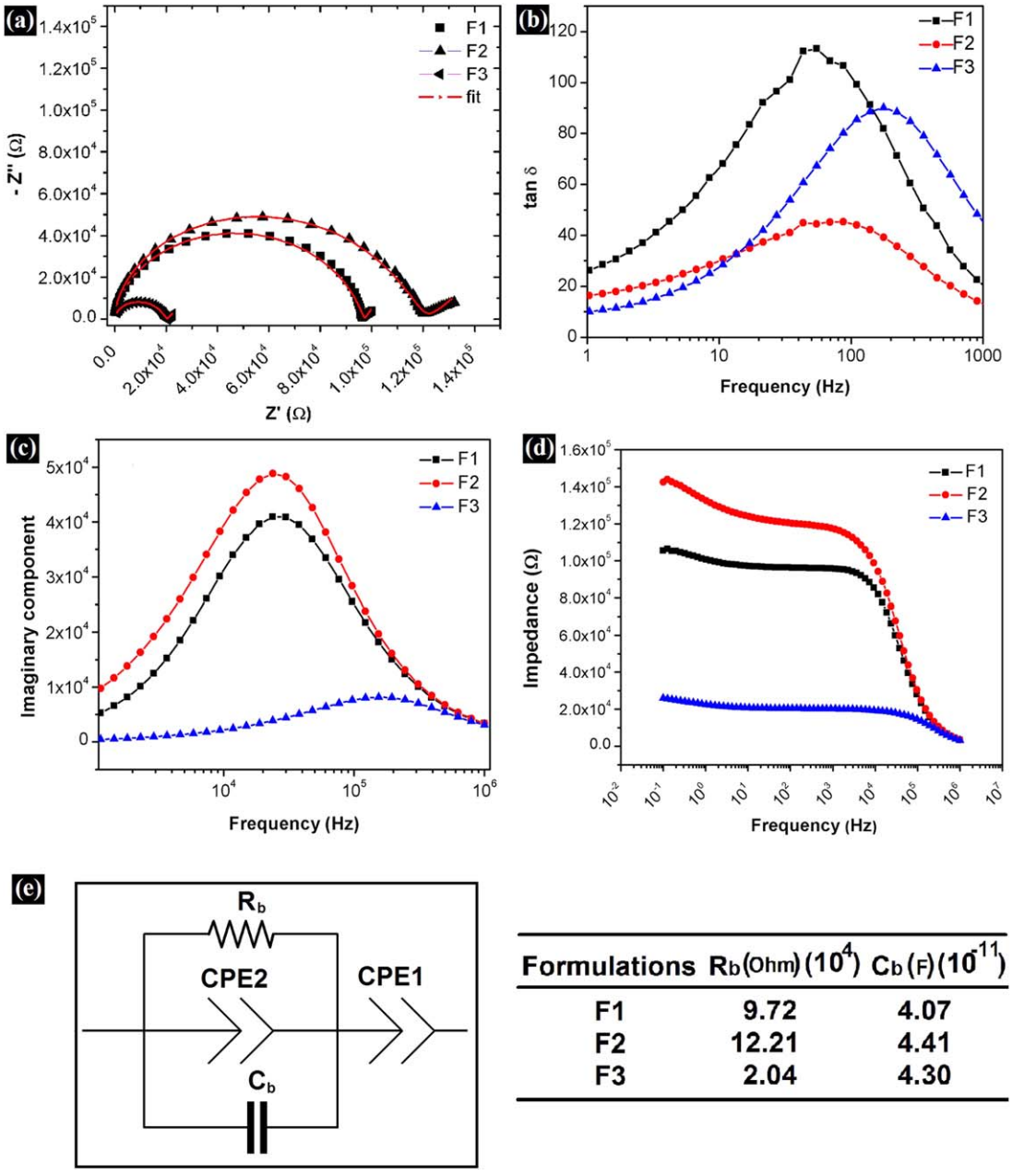

Formulations	Rb(Ohm)(10^4)	Cb(F)(10^{-11})
F1	9.72	4.07
F2	12.21	4.41
F3	2.04	4.30

Figure 5. Electrical properties of organogels (a) Nyquist plot, (b) frequency vs. tan δ, (c) frequency vs. imaginary component, (d) frequency vs. impedance, and (e) equivalent circuit diagram with R_b and C_b values obtained after fitting the impedance data. [Color figure can be viewed in the online issue, which is available at wileyonlinelibrary.com.]

Thermal Studies

Figure 4 shows the DSC thermograms of the organogels. The thermograms of the organogels have shown a single broad endothermic peak. This was due to the evaporation of the water molecules. Though the organogels have shown single endothermic peak, the position of the peak was different. This may be due to the extent of intermolecular hydrogen bonding among the organogel components. The occurrence of the endothermic

Table IV. Mechanical Properties Obtained from the Stress Relaxation Studies

Formulations	WR (g·sec)	F_0 (g)	F_r (g)	% Relaxation	k_1	k_2	S
F1	193.25	12.21	4.91	39.13	0.1361	0.0001	0.3906
F2	195.55	11.68	5.44	45.45	0.1518	0.0001	0.3892
F3	531.59	35.16	12.07	36.98	0.1258	0.0001	0.3897

Table V. Mechanical Properties Obtained from the Gel Strength, Spreadability Studies, and Backward Extrusion (Be) Studies

Formulations	Firmness (g)	Stickiness (g)	Adhesiveness (g·sec)	Cohesiveness (g·sec)	Index of viscosity (g·sec)
F1	146.50 ± 2.5	−220.8 ± 3.7	−83.65 ± 2.4	219.40 ± 3.2	759.46
F2	153.82 ± 3.2	−258.22 ± 3.9	−92.05 ± 3.6	209.93 ± 2.7	685.56
F3	436.83 ± 2.8	−655.90 ± 1.9	−229.55 ± 2.2	1415.60 ± 3.6	1373.13

peak temperature (T_p) was highest for F3 followed by F2 and F1. This may be due to the structural variations of organogels as was evident from the XRD studies, which suggested that the crystallinity of F3 was highest followed by F2 and F1. In general, the presence of endothermic peak at higher temperatures indicates higher thermal stability of the formulations.[34]

Impedance Analysis

Figure 5 shows the complex impedance spectra (Nyquist plot) of the organogels. The plot showed two distinct regions in all the gels. The high frequency region contained a slightly depressed semi-circle which can be attributed to the bulk effect of electrolytes. The low frequency region showed a non-vertical spike which can be attributed to the roughness of the electrode-sample interface.[39] The intercept of the semicircle on the real axis gives bulk resistance of the materials from the Nyquist plot.[40] There was a decrease in the bulk resistance (R_b) of the organogels in the following order F2> F1>>F3. The results may be explained by the fact that higher proportions of water resulted in a corresponding decrease in the R_b. The tan δ plot of the organogels has shown a single relaxation peak. This may be due to the ionic transport process in the bulk phase.[41] The impedance profile showed F2 had highest impedance followed by F1 and F3. The result was in accordance with the bulk resistance of the organogels obtained from the Nyquist plot. The results showed that there was a decrease in the impedance of the organogels with the increase in the frequency thereby suggesting a capacitive dominant behavior of the organogels. The relaxation time of the organogels was calculated from the imaginary component profile using the following equation:

$$2\pi f_{max}\,\tau_m = 1 \quad (1)$$

where,

f_{max} = frequency at Z" max.

τ_m = Relaxation time

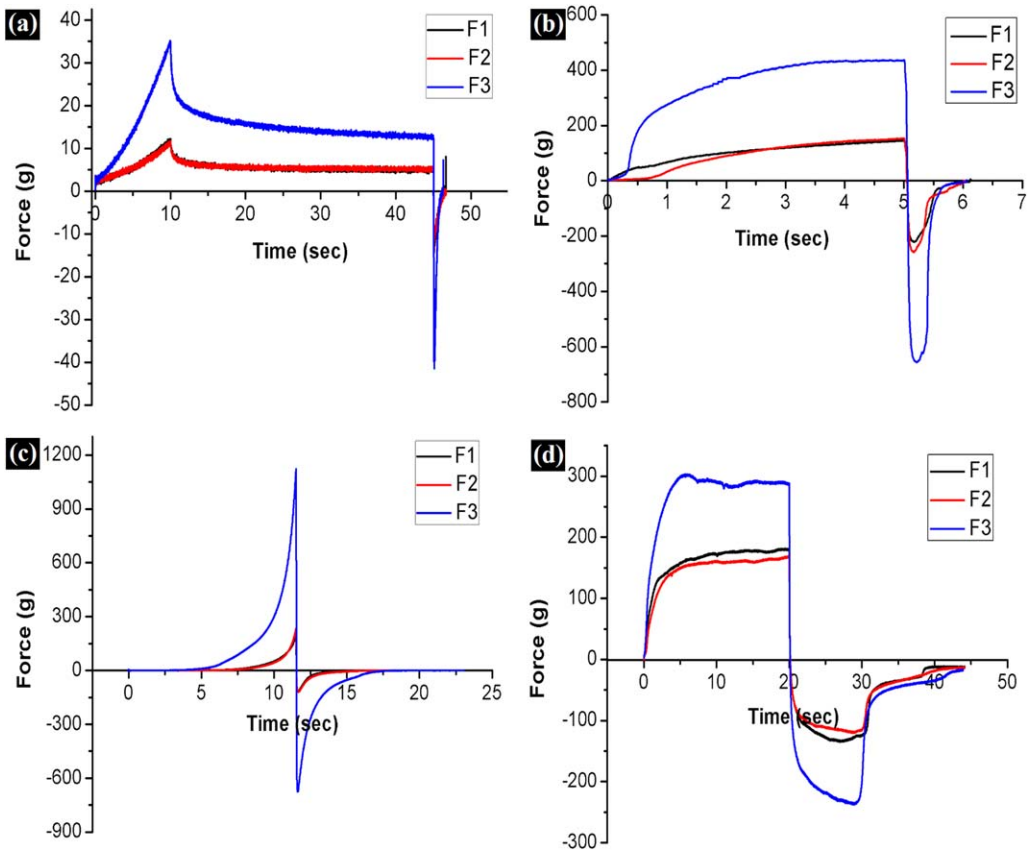

Figure 6. Textural studies of organogels (a) stress relaxation studies, (b) gel strength studies, (c) spreadability studies, and (d) backward extrusion studies. [Color figure can be viewed in the online issue, which is available at wileyonlinelibrary.com.]

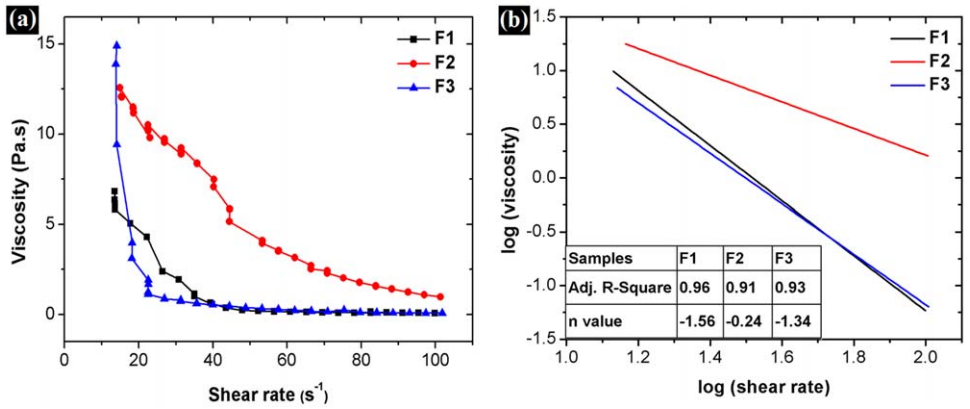

Figure 7. (a) Pseudoplastic behavior of the organogels and (b) modified power law fitting of the organogels. [Color figure can be viewed in the online issue, which is available at wileyonlinelibrary.com.]

It was observed that the relaxation time (τ_m) of F3 (29,891 Hz^{-1}) was maximum compared with F1 (3908 Hz^{-1}) and F2 (3848 Hz^{-1}). This might be explained by the fact that an increase in aqueous phase lead to the increased mobility of the charged particles within the gel systems.[42]

The modelling of the Nyquist plot was done by proposing an electrical equivalent circuit [Figure 5(e)]. The inhomogeneity of the system is counterbalanced by adding a constant phase (CPE) element in the equivalent circuit. Two CPE elements have been introduced in the equivalent circuit which were named as CPE1 and CPE2.[43] The proposed electrical circuit contained a parallel combination of bulk resistance, bulk capacitance and a CPE element (CPE2) which represented the semicircle (bulk effects). An another CPE element (CPE1) was added in series to represent the spike obtained as a result of electrode–sample interface.[39] The data was fitted using commercially available computer software Z SimpWin. The red lines as shown in Figure 5(a) indicated a good fit data. The bulk resistance and bulk capacitance (C_b) obtained after fitting the impedance data are shown in Figure 5(e).

Mechanical Analysis

The mechanical properties of the organogels were analyzed by stress relaxation (SR), gel strength, spreadability studies and backward extrusion (BE) studies (Table IV and V, Figure 6). The SR profiles of the organogels were determined using a cone probe, made of perpex. The cone was allowed to move a distance of 10 mm after a trigger force of 5 g. The maximum force at the distance of 10 mm was noted as F_0. The probe was held at the same position for 30 sec. During this time, the deforming force due to the stress applied started dissipating. The force sensed by the probe at the end of 30 sec was regarded as F_{30}. The percent decrease in the force due to hold time was calculated as the % SR.[44,45] The area under the F_0 and F_{30} curve was regarded as work on relaxation (WR). The results of the study have been tabulated in Table IV. % SR is a measure of molecular rearrangement of the organogel components after the stress is applied. The %SR was found to be highest in F3 followed by F1 and F2, respectively. The WR was found to be highest in F3 whereas the WR of F1 and F2 were found to be similar. This suggested that the firmness of F3 was much higher compared with F1 and F2. Similar finding was also evident from the gel strength studies.

The stress relaxation profile was further analyzed by modified Peleg's equation.[46]

$$\frac{(F_0 - F(t))t}{F_0} = k_1 + k_2 t \quad (2)$$

where, F_0 is the maximum force attained when a specific force is applied; k_1 and k_2 are the Peleg's constants which indicates the initial rate and extent of the relaxation, respectively.

k_1 provides information regarding the initial force decay rate whereas k_2 provides information regarding the overall relaxation. The normalized stress relaxation data was plotted against time and fitted linearly ($r^2 > 0.995$). The initial rate of the relaxation (k_1) was lower in the organogels with higher DW/SM ratio. It was in the order of F3> F1> F2. The k_2 values of the organogels was almost equal. The viscoelastic properties of the organogels were quantified by calculating the area under the normalized stress relaxation curve (S). The S value was found to be ~0.48 (Table IV) which suggested viscoelastic fluid nature of the organogels.[47]

The highest force required to penetrate/deform the organogels is regarded as the firmness of the organogels.[48] The firmness of F3 was much higher compared with F1 and F2. The firmness of F1 and F2 was almost comparable (Table V). The firmness of F3 may be associated with the higher degree of intermolecular hydrogen bonding in F3 due to highest DW/SM-PM ratio as against F1 and F2. The DW/SM ratio was similar in F1 and F2. Because of this, the firmness of F1 and F2 was expected to be similar. The maximum negative force recorded during retraction of the probe is regarded as the stickiness and the area under the negative curve is the adhesiveness of the gels.[49,50] The stickiness and adhesiveness of F3 was highest compared with F1 and F2.

Spreadability is a measure of how easily a formulation can be spread. As a matter of fact, the area under the positive peak (cohesiveness) is inversely proportional to the spreadability. The results suggested that F3 was least spreadable, whereas the spreadability of F1 and F2 were comparable.

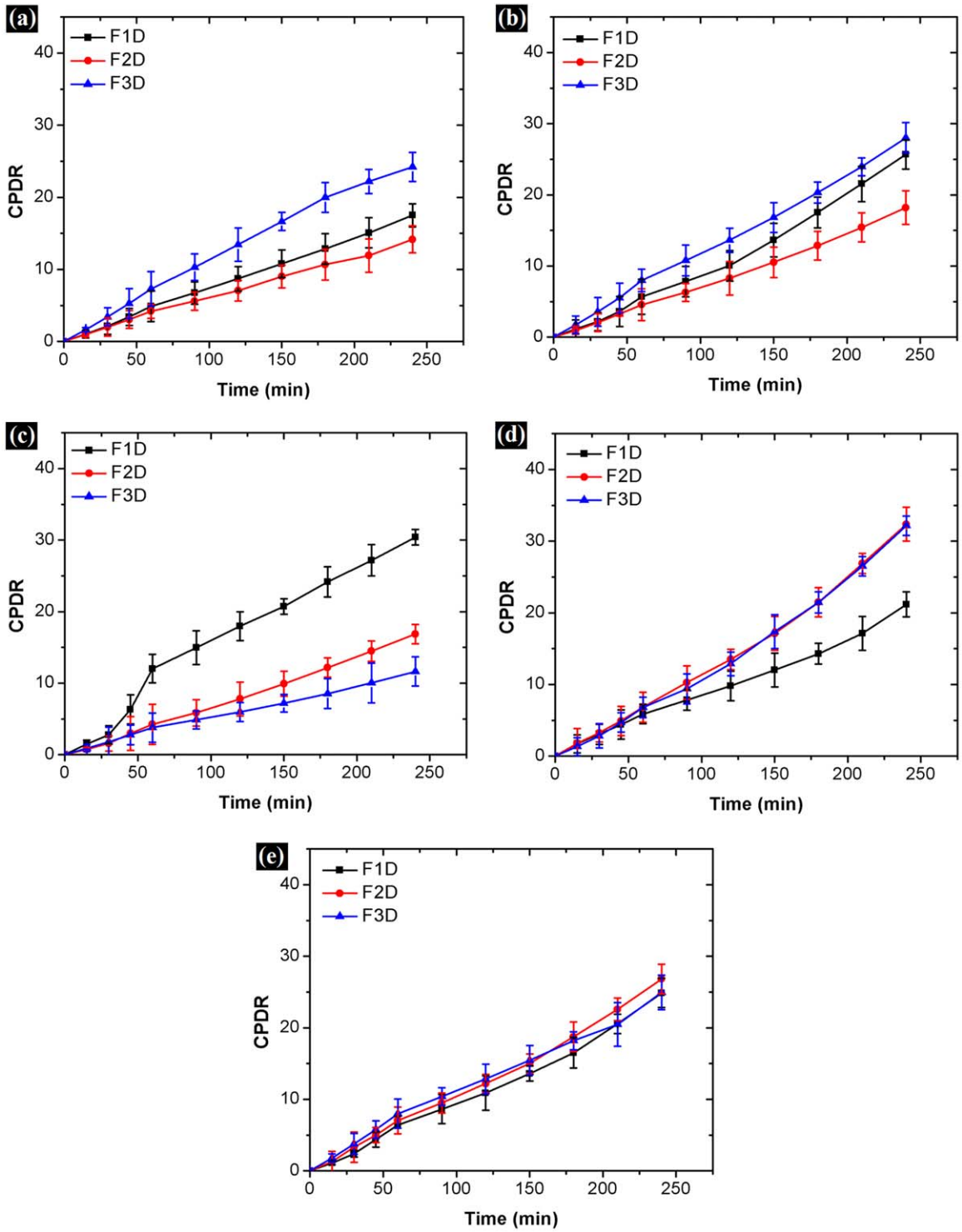

Figure 8. The *in vitro* drug delivery profiles under (a) passive diffusion and (b) SN, (c) SQ (d) SNH, and (f) SQH wave forms. [Color figure can be viewed in the online issue, which is available at wileyonlinelibrary.com.]

The BE studies were conducted to have an insight on the index of viscosity of the organogels. The index of viscosity of the organogels was calculated from the area under the negative peak.[51] F3 was found to be having higher viscosity index which was followed by F1 and F2 (Table V).

Viscosity Studies

The viscosity profile (Figure 7) of the organogels suggested shear-thinning property, i.e. the viscosity of the organogels decreased with the increase in the shear rate. It was observed that at low shear rates, F3 had the highest dynamic viscosity

Table VI. The Mean CPDR and % Increase in CPDR Values of Organogels Due to Iontophoresis

	CPDR			% Increase in CPDR		
Type of waveform	F1D	F2D	F3D	F1D	F2D	F3D
Passive diffusion	17.50	14.16	24.2	—	—	—
SN	25.67	18.18	28.01	46.68	28.39	15.74
SQ	30.40	16.87	31.64	73.71	19.13	30.74
SNH	21.16	32.36	32.16	20.91	128.53	32.89
SQH	24.87	26.82	34.95	42.11	89.40	44.42

compared with F2 and F1, respectively. The index of viscosity calculated from BE studies also suggested that the viscosity was highest in F3. The shear-thinning property may be attributed to the destruction of the networked structures at higher shear rates. The flow behavior of the organogels was predicted by calculating the flow behavior index (n) using Ostwald-de wale modified power law.[52] The 'n' value of the organogels was found to be <1, suggesting pseudoplastic flow behavior of the organogels [Figure 7(b)].

The Herschel–Bulkley model [eq. (4)] is used to calculate the yield stress required for a formulation.

$$\tau = \tau_c + K\gamma^n \quad (3)$$

where, τ is the shear stress; τ_c is the yield stress, k is the consistency, n is the flow index, and γ is the deformation rate or shear rates.

The yield stress is considered as an indirect representation of the strength of the formulations. Similar to the bulk resistance, the yield stress of the organogels were found to be in the order of F2 (1.44) > F1 (1.32) > F3 (1.18). The organogels with higher DW/SM ratio showed lower yield stress values. This suggested that the organogels containing higher water content resulted in lower yield stress.

In Vitro Drug Release Studies

The *in vitro* drug release profiles from the organogels have been shown in Figure 8. The height and diameter of the donor chamber was 3.62 and 2.5 cm, respectively. 15 g of the drug loaded organogel was used for the study. The drug release studies suggested that the cumulative percent drug release (CPDR) from the organogels was higher when electrical current was applied compared with the passive diffusion (Table VI). Percentage increase in CPDR due to the application of different current wave forms has also been tabulated in Table VI. Under the experimental conditions, the modified waveforms (SNH, SQH) have shown higher % increase in CPDR than the native waveforms when compared with the passive drug release studies. In general, the pulsed iontophoresis (SNH, SQH) prevent the electrode polarization which might have facilitated the higher drug movement.[53] In case of SN and SQ waveforms, the frequent

Table VII. The Drug Release Kinetics of Organogels

					KP model	
Wave form	Sample code	Zero order (r^2)	Higuchi (r^2)	Best fit	*n*	Type of flow
Pas	F1D	0.98	0.98	Zero order	0.92	Case-II transport
	F2D	0.99	0.87	Zero order	0.94	Case-II transport
	F3D	0.99	0.87	Zero order	1.00	Case-II transport
SN	F1D	0.99	0.81	Zero order	1.09	Case-II transport
	F2D	0.99	0.86	Zero order	1.02	Case-II transport
	F3D	0.99	0.88	Zero order	0.98	Case-II transport
SQ	F1D	0.99	0.80	Zero order	1.2	Case-II transport
	F2D	0.99	0.84	Zero order	1.13	Case-II transport
	F3D	0.97	0.91	Zero order	0.89	Case-II transport
SNH	F1D	0.98	0.91	Zero order	0.84	Case-II transport
	F2D	0.99	0.84	Zero order	1.00	Case-II transport
	F3D	0.99	0.81	Zero order	1.10	Case-II transport
SQH	F1D	0.99	0.86	Zero order	1.08	Case-II transport
	F2D	0.99	0.88	Zero order	1.02	Case-II transport
	F3D	0.93	0.90	Zero order	0.93	Case-II transport

and continuous change in electrode polarity might have resulted in the lower drug release.

The drug release kinetics was predicted by best-fit model estimation. Data fitting was performed upon the 60% of the total drug released.[54] The results showed that the release of the drug followed Zero-order kinetics under both passive and active conditions (Table VII). This suggested that the release of the drugs was predominantly by diffusion and the release was concentration independent under the experimental conditions.[55,56] The results indicated that the application of electrical potential of different waveforms did not alter the mechanism of drug release but only facilitated the active diffusion of the drug.

The Korsmeyer-Peppas (KP) release exponent (n) value was calculated from the slope of the KP model (Table VII). The results indicated Case-II or super Case-II transport phenomenon. Usually, this kind of transport phenomenon is reported when the diffusion of the drugs is much faster compared with the relaxation of the polymer molecules of the delivery matrices.[57]

CONCLUSION

The current study reports the physical and electrical characterization of the Tween 80-Span 80 and sunflower oil based organogels. The properties of the organogels were dependent on the composition of the organogels. An increase in the gelator concentration increased the physical properties of the organogels. On the other hand, an increase in the water concentration resulted in the decrease in the physical properties. The electrical properties of the organogels were improved with the increase in the water concentration. The iontophoretic drug delivery suggested that the rate of release of the drug from the matrix was a complex phenomenon dependent on the composition of the organogels and the waveform pattern of the electrical potential applied. Though the results are preliminary, the results of the *in vitro* drug release studies suggested that the developed organogels may be tried as carriers for iontophoretic drug delivery.

ACKNOWLEDGMENTS

The authors acknowledge the instrumental facilities provided by National Institute of Technology, Rourkela (NIT-R), India. The authors extend their gratitude toward the Department of Biotechnology, Government of India for sanctioning and funding the project (BT/PR14282/PID/06/598/2010).

REFERENCES

1. Bíró, T.; Tóth, B. I.; Haskó, G.; Paus, R.; Pacher, P. *Trends Pharmacol. Sci.* **2009**, *30*, 411.
2. Hu, L.; Batheja, P.; Meidan, V.; Michniak-Kohn, B. B. In Handbook of Non-Invasive Drug Delivery Systems; Vitthal, S. K., Ed.; William Andrew Publishing: Boston, **2010**, p 95.
3. Mutalik, S.; Parekh, H.; Anissimov, Y.; Griceand, J.; Roberts, M. *Skin Pharmacol. Physiol.* **2013**, *26*, 127.
4. Wang, K.; Xu, X.; Liu, T.; Fu, S.; Guo, G.; Gu, Y.; Luo, F.; Zhao, X.; Wei, Y.; Qian, Z. *Carbohydr. Polym.* **2010**, *79*, 755.
5. Fan, Q.; Sirkar, K. K.; Michniak, B. *J. Membr. Sci.* **2008**, *321*, 240.
6. Singh, P.; Maibach, H. I. *Crit. Rev. Ther. Drug Carrier Syst.* **1994**, *11*, 161.
7. Kalluri, H.; Banga, A. K. *AAPS PharmSciTech* **2011**, *12*, 431.
8. Nicoli, S.; Ferrari, G.; Quarta, M.; Macaluso, C.; Santi, P. *Eur. J. Pharm. Sci.* **2009**, *36*, 486.
9. Tomoda, K.; Terashima, H.; Suzuki, K.; Inagi, T.; Terada, H.; Makino, K. *Colloids Surf. B* **2011**, *88*, 706.
10. Song, K.; Ha, U.; Lee, J.; Bong, K.; Yoo, H. J. Solid-State Circuits Conference Digest of Technical Papers (ISSCC), 2013 IEEE International, 2013, p 98.
11. Jin, J. N.; Liu, Z. P.; Li, Y.; Yin, T. *Chin. Med. Equip. J.* **2009**, *9*, 4.
12. Guo, B.; Finne-Wistrand, A.; Albertsson, A. C. *Chem. Mater.* **2011**, *23*, 1254.
13. Fallows, S. J.; Garland, M. J.; Cassidy, C. M.; Tunney, M. M.; Singh, T. R. R.; Donnelly, R. F. *J. Photochem. Photobiol. B* **2012**, *114*, 61.
14. Almeida, H.; Amaral, M. H.; Lobão, P.; Lobo, J. M. S. *J. Pharm. Pharm. Sci.* **2012**, *15*, 592.
15. Kanjilal, B.; Dasgupta, R.; Banthia, A. K. *Int. J. Plast. Technol.* **2011**, *15*, 19.
16. Bera, P.; Alam, A. A.; Arora, N.; Tibarewala, D. N.; Basak, P. AIP Conference Proceedings, **2013**, p 1223.
17. Hajare, A. A.; Mali, M. N.; Dange, A. S.; Sarvagod, S. M.; Patwardhan, S. V.; Kurane, S. T. *Res. J. Pharm. Dosage Forms Technol.* **2009**, *1*, 280.
18. Niamlang, S. *Bull. Am. Phys. Soc.* **2009**, *54*, 1.
19. Shah, D. K.; Sagiri, S. S.; Behera, B.; Pal, K.; Pramanik, K. *J. Appl. Polym. Sci.* **2013**, *129*, 793.
20. Moniruzzaman, M.; Sahin, A.; Winey, K. I. *Carbon* **2009**, *47*, 645.
21. Singh, V. K.; Pal, K.; Pradhan, D. K.; Pramanik, K. *J. Appl. Polym. Sci.* **2013**, *130*, 1503.
22. Bhattacharya, C.; Kumar, N.; Sagiri, S. S.; Pal, K.; Ray, S. S. *J. Pharm. Bioallied Sci.* **2012**, *4*, 155.
23. Singh, V. K.; Ramesh, S.; Pal, K.; Anis, A.; Pradhan, D. K.; Pramanik, K. *J. Mater. Sci. Mater. Med.* **2013**, *25*, 703.
24. Shah, D. K.; Sagiri, S. S.; Behera, B.; Pal, K.; Pramanik, K. *J. Appl. Polym. Sci.* **2013**, *129*, 793.
25. Khade, S. M.; Behera, B.; Sagiri, S.; Singh, V.; Thirugnanam, A.; Pal, K.; Ray, S.; Pradhan, D.; Bhattacharya, M. *Iranian Polym. J.* **2014**, *23*, 171.
26. Singh, V. K.; Sagiri, S. S.; Pal, K.; Khade, S. M.; Pradhan, D. K.; Bhattacharya, M. K. *J. Appl. Polym. Sci.* **2014**, *131*, 40445.
27. Pal, K.; Singh, V. K.; Anis, A.; Thakur, G.; Bhattacharya, M. K. *Polym-Plast. Technol. Eng.* **2013**, *52*, 1391.
28. Mallick, S.; Sagiri, S.; Singh, V.; Pal, K.; Pradhan, D.; Bhattacharya, M. *Polym. Plast. Technol. Eng.* **2014**, *53*, 700.
29. Pradhan, S.; . Sagiri, S. S; Singh, V. K.; Pal, K.; Ray, S. S.; Pradhan, D. K. *J. Appl. Polym. Sci.* **2014**, 131, 39979.
30. Vamathevan, V.; Amal, R.; Beydoun, D.; Low, G.; McEvoy, S. *J. Photochem. Photobiol. A* **2002**, *148*, 233.

31. Pal, K.; Banthia, A.; Majumdar, D. *AAPS PharmSciTech.* **2007**, *8*, E142.
32. Bhattacharya, C.; Pal, V.; Kumar, N.; Sagiri, S.; Ray, S. *J. Pharm. Bioallied Sci.* **2012**, *4*, 155.
33. Singh, V. K.; Pal, K.; Pradhan, D. K.; Pramanik, K. *J. Appl. Polym. Sci.* **2013**.
34. Sagiri, S. S.; Behera, B.; Pal, K.; Basak, P. *J. Appl. Polym. Sci.* **2012**.
35. Behera, B.; Sagiri, S. S.; Pal, K.; Srivastava, A. *J. Appl. Polym. Sci.* **2013**, *127*, 4910.
36. Vintiloiu, A.; Leroux, J. C. *J. Controlled Release.* **2008**, *125*, 179.
37. Hurle, D. T. Handbook of crystal growth, Elseiver: North Holland, **1993**.
38. Even, W. R.; Crocker, R. W.; Hunter, M. C.; Yang, N. C. Headley, *T. J. J. Non-Cryst. Solids.* **1995**, *186*, 191.
39. Pradhan, D. K.; Choudhary, R.; Samantaray, B.; Thakur, A. K.; Katiyar, R. *Ionics.* **2009**, *15*, 345.
40. Pradhan, D. K.; Samantaray, B.; Choudhary, R. N. P.; Thakur, A. K. *Ionics.* **2005**, *11*, 95.
41. Padmasree, K.; Montalvo-Lozano, R.; Montemayor, S.; Fuentes, A. *J. Alloys Compd.* **2011**, *509*, 8584.
42. Yoshioka, S.; Aso, Y.; Otsuka, T.; Kojima, S. *J. Pharm. Sci.* **1995**, *84*, 1072.
43. Pradhan, D. K.; Samantaray, B.; Choudhary, R.; Thakur, A. K. *J. Mater. Sci. Mater. Electron.* **2006**, *17*, 157.
44. Bhattacharya, S. *J. Food Eng.* **2010**, *97*, 539.
45. Wu, Y.; Cui, W.; Eskin, N. A. M.; Goff, H. D. *Carbohydr. Polym.* **2011**, *84*, 984.
46. Peleg, M. *J. Food Sci.* **1979**, *44*, 277.
47. Bellido, G. G.; Hatcher, D. W. *J. Food Eng.* **2009**, *92*, 29.
48. Turgeon, S. L.; Beaulieu, M. *Food Hydrocolloids.* **2001**, *15*, 583.
49. Fiszman, S. M.; DamÁSio, M. H. *J. Texture Stud.* **2000**, *31*, 69.
50. Tamburic, S.; Craig, D. Q. M. *Eur. J. Pharm. Biopharm.* **1997**, *44*, 159.
51. Sadough, S. A.; Rahmani, M. R.; Pouyafar, V. *Trans. Nonferrous Met. Soc. China.* **2010**, *20*, 906.
52. Yu, T.; Malcolm, K.; Woolfson, D.; Jones, D. S.; Andrews, G. P. *Expert Opin. Drug Deliv.* **2011**, *8*, 1309.
53. Nishimura, T.; Akimoto, M.; Miyazaki, M.; Nomoto, M.; Miyakawa, M. *Session 2A7* **2010**, 315.
54. Dash, S.; Murthy, P. N.; Nath, L.; Chowdhury, P. *Acta. Pol. Pharm.* **2010**, *67*, 217.
55. Hill, A.; Geißler, S.; Weigandt, M.; Mäder, K. *J. Controlled Release.* **2012**, *158*, 403.
56. Khunt, D. M.; Mishra, A. D.; Shah, D. R. *Int. J. Pharm. Tech. Res.* **2012**, *4*, 1332.
57. Daniel-da-Silva, A. L.; Moreira, J.; Neto, R.; Estrada, A. C.; Gil, A. M.; Trindade, T. *Carbohydr. Polym.* **2012**, *87*, 328.